ELSEVIER

PII: S0032-3861(97)00593-4

Polymer Vol. 39 No. 13, pp. 2903–2915, 1998

0032-3861/98/$19.00+0.00

Kinetics of pressure-induced phase separation (PIPS) from polymer solutions by time-resolved light scattering. Polyethylene + *n*-pentane

Wenhao Zhuang and Erdogan Kiran*
Department of Chemical Engineering, University of Maine, Orono, ME 04469-5737, USA
(Received 2 March 1997; revised 8 July 1997; accepted 16 July 1997)

Kinetics of pressure-induced phase separation (PIPS) in solutions of polyethylene + *n*-pentane at high pressures have been investigated using a novel experimental system which permits imposing controlled, multiple rapid (and repetitive) pressure quenches of different penetration depths into the region of immiscibility of the system. The evolution of new phase formation is monitored by time-resolved light scattering using a fibre optic scattering cell as a function of the depth of penetration into the two-phase regions. It is shown that the rate of change in the scattered light intensities increases with quench depth, becoming very fast and eventually reaches an apparent limiting value for quenches below a characteristic penetration depth. Determination of these quench pressures below which phase separation is extremely rapid identifies a kinetic phase separation boundary below the binodal pressures which is of practical significance. This is because pressure-induced phase separation by rapid expansion is an important step in processing of materials such as polymers with near- and supercritical fluids. The results are shown for liquid–liquid phase separation for polyethylene solutions of two different molecular weights (108 000 and 16 400) in *n*-pentane subjected to pressure quenches as deep as 10 MPa.

(Keywords: pressure-induced phase separation; polyethylene + *n*-pentane; time-resolved light scattering)

INTRODUCTION

The literature on phase separation in polymer systems is rich and includes a variety of experimental techniques that try to simulate the different conditions encountered in practice. Indeed, a homogeneous polymer solution may undergo phase separation as a result of a change in temperature[1–5], pressure[6–13], composition (which may come about from addition of a non-solvent[14–17] or removal of the solvent as in solvent evaporation). Phase separation may also arise from changes due to chemical reactions as in polymerisation[18,19], or from changes in the external fields or the hydrodynamics of the system such as changes in applied shear[20,21].

Among these, solvent and thermal-induced phase separation are by far the most common techniques that are employed. However, due to the growing interest in supercritical fluid based processes where pressure reduction is an integral step in the recovery of the end-product (or the solvent), there is now much interest in pressure as a parameter in phase separation from polymer solutions[6–9]. Pressure-induced phase separation (PIPS) offers a special advantage in that pressure can be changed very rapidly in the bulk of the solution and the two-phase regions can be entered faster than would be possible by other techniques.

The essential features of PIPS are described in *Figure 1*. This is a pressure-composition phase diagram showing the binodal (the curve that separates the stable one-phase region from the region in which two phases coexist in equilibrium) and the spinodal (which divides the two-phase region into metastable and unstable portions) boundaries, and the stable, metastable and the unstable regions. This is an idealised diagram in that in real systems, due to polydispersity of polymers, the binodal and spinodal curves do not necessarily merge at the maximum of the binodal—they merge at a higher concentration. The pressure reduction paths AB and A″B″ represent phase separation in the metastable region by nucleation and growth mechanism. In relatively dilute solutions (path AB) polymer-rich phase nucleates in a solvent-rich continuous phase, whereas in a concentrated solution (path A″B″), polymer-lean phase nucleates in a polymer rich-phase which is continuous. These are characterised by the existence of continuous-phase, dispersed-phase morphology. The pressure reduction path A′B′ represents phase separation by spinodal decomposition. Here, there is no thermodynamic barrier to phase growth and the solution which is at its critical concentration undergoes spontaneous and continuous phase separation with the formation of co-continuous phases in the early stages of phase separation. In the later stages of phase separation, the bicontinuity of the phases may however be lost through ripening (coarsening) as the system seeks to minimise its free energy by minimising interfacial area unless the structure is frozen due to gelation or vitrification during phase separation. The co-continuous domain structures may break into droplets. It should be noted that for these pressure reduction paths from an initial pressure P_i to a final pressure of P_f, the final equilibrium compositions of the two phases that are formed are all the same, ϕ_{Ib} and ϕ_{IIb}. The ratio of the equilibrium phase for each case is however different (and can be determined by the lever rule).

Figure 2 illustrates the different morphologies that develop during phase separation and when the final equilibrium stage is reached. The kinetics of phase separation processes however may prevent reaching the final equilibrium state and the intermediate non-equilibrium

* To whom correspondence should be addressed

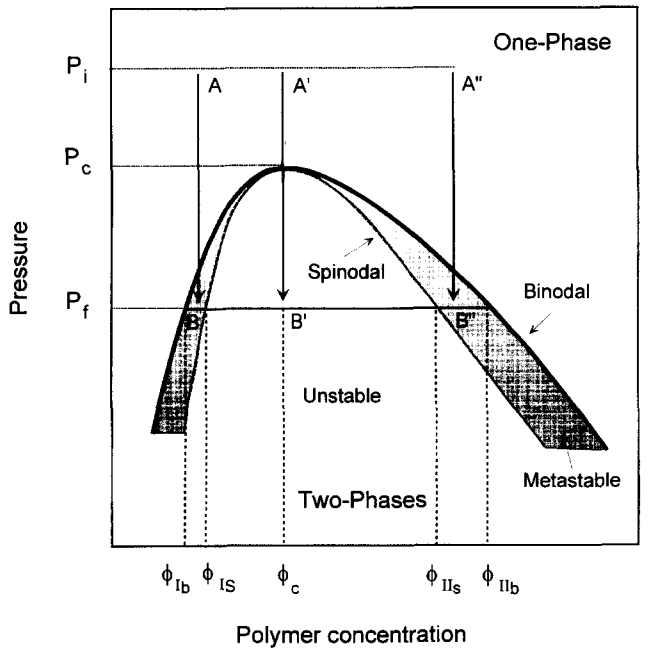

Figure 1 Schematic representation of pressure-induced phase separation in the pressure-composition phase diagram. The binodal and the spinodal envelopes separate the stable one-phase, unstable two-phase regions. The region between the spinodal and the binodal (shaded area in the figure) is the metastable region. Three different pressure reduction paths (AB, A'B' and A"B") are shown for solutions at three different polymer concentrations, all starting at an initial pressure of P_i in the one-phase homogeneous region and ending at a final pressure of P_f in the two-phase regions. These paths, even though different, all result in the same equilibrium phase compositions ϕ_{Ib} and ϕ_{IIb}. New phase formation proceeds by Nucleation and Growth mechanism when metastable regions are entered (paths AB, and A"B"), and by Spinodal Decomposition mechanism when the unstable regions are entered (path A'B') upon reduction in pressure

states may be locked-in as in vitrification. From *Figure 1* and *Figure 2*, it is easy to see how pressure-induced phase separation may lead to different morphologies, ranging from powders, to porous structures of different pore size and distributions. Clearly, not only the final thermodynamic state, but also the kinetics of phase separation and the time scale involved in new phase formation are of great technological interest.

Experimental and theoretical studies on the kinetics of phase separation have been mostly reported for polymer blends subjected to a temperature quench[2,3,21–24]. In polymer blends kinetics are easier to follow because of the high viscosity and low diffusivity, and thus the longer time scales that are involved. For polymer solutions, the dynamics of phase separation and the early-stage structure development are fast, and for deep quenches time scales may be extremely short, making these systems experimentally more difficult to study if not inaccessible. *Table 1* is a summary of all the available literature on the kinetics of phase separation from polymer solutions involving a polymer plus a solvent. Many of these studies report the consequences of temperature-induced phase separation (TIPS). Outside our laboratory, only two other studies have been reported on the kinetics of pressure-induced phase separation in polymer solutions with measurements on the time scales of phase separation. Kuwahara *et al.*[38,39] have reported on the dynamics of spinodal decomposition in polydimethylsiloxane + diethyl carbonate subjected to a shallow pressure quench of 0.04–0.074 MPa near atmospheric pressure. Kojima *et al.* have reported on the consequences of shallow pressure-quenches (*ca.* 0.03–0.05 MPa) from an initial pressure of about 5 MPa for a 1.5% solution of polypropylene (M = 355 000, PDI = 6.5) in trichlorfluoromethane. Based on time-resolved scattered light intensities, the authors concluded that phase separation proceeded by spinodal decomposition for 0.05 MPa quench below the phase boundary at 452 K, but by nucleation and growth for a shallower quench depth of 0.03 MPa[37]. In our previous publications[6,7] we reported on the time-evolution of scattered light intensities in solutions of polystyrene + pentane for rapid deep quenches into the region of immiscibility from high

Table 1 Literature on kinetics of phase separation in polymer solutions

System	Quench mode/measurement technique	Reference
Poly(2,6-dimethyl-1,4-phenylether) (PPO) + caprolactam	TIPS/OM	Smolders *et al.* [25]
Polystyrene + diisodecyl phthalate	TIPS/OM	Nojima *et al.* [26]
Styrene oligomers + *e*-caprolactone	TIPS/OM	Tanaka *et al.* [27,28]
Polystyrene + cyclohexane	TIPS/TR-LS	Lal and Bansil [29]
Polystyrene + cyclohexane	TIPS/SEM, BET,	Aubert [30,31]
Poly(*p*-phenylenebezobisoxazole) (PBO) + methanesulfonic acid	SIPS/TR-LS	Nelson and Soane [5]
Polystyrene + diethyl malonate	TIPS/M	Tanaka [32]
Polystyrene + cyclohexane; PS + diethyl malonate	TIPS/SEM/POR	Song and Torkelson [33]
Isotactic polypropylene + diphenyl ether	TIPS/OM	McGuire *et al.* [34]
Polymer + liquid crystal	SIPS/LS	Kikuchi *et al.* [35]
Poly(diisopropyl fumarate) + E8		
Polystyrene + dioctylphthalate	TIPS/ SAXS	Xie *et al.* [36]
Polypropylene + trichlorofluoromethane	PIPS/LS	Kojima *et al.* [37]
Polydimethylsiloxane + diethyl carbonate	PIPS	Kuwahara *et al.* [38,39]
Polystyrene + pentane	PIPS/TR-LS	Kiran [6]; Kiran and Zhuang [7]; Zhuang [40]
Polyethylene + pentane	PIPS/TR-LS	Zhuang and Kiran[8,9]; Zhuang [40]
Polystyrene + methyl cyclohexane	PIPS/TR-LS	Kiran [13]; Xiong [62]

TIPS = temperature-induced phase separation; OM = optical microscopy; TR-LS = time-resolved light scattering; SIPS = solvent induced phase separation; SEM = scanning electron microscopy; SAXS = small angle X-ray scattering; LS = light scattering; POR = porosimetry; PIPS = pressure-induced phase separation.

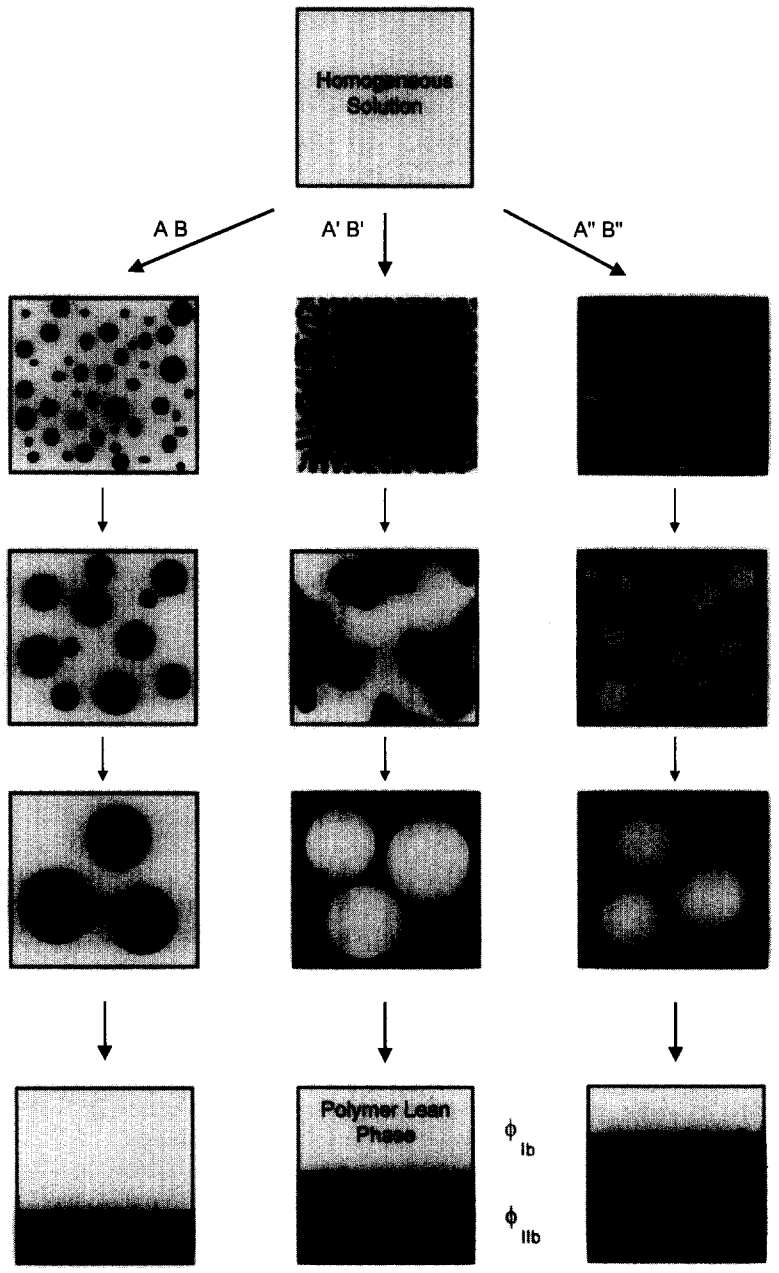

Figure 2 Schematic representation of the different morphologies (particles, interconnected network, porous matrix) that are formed and their evolution (coarsening process) with time upon phase separation depending upon the phase separation path followed, as described in *Figure 1*. They all reach a final two-phase equilibrium state with identical phase compositions, but different phase-volume ratios. Under certain circumstances, the kinetics of phase separation may prevent reaching the final equilibrium state, thereby locking-in the non-equilibrium states leading to different morphologies

pressures. These studies were the very first investigations of their kind in which rapid deep-quenches (up to about 10 MPa) have been employed in a repetitive manner and have shown that the time-scale of new phase formation indeed becomes very short for deep quenches. Recently, we also reported[8,9] on the time scale and rate of phase separation for polyethylene (M_w = 16400) + pentane system at 150°C for concentrations in the range of 1–15% by mass subjected to different pressure quenches ranging from shallow to deep quenches.

In the present paper, we report on the details of a relatively new technique based on time-resolved light scattering using a fibre-optic cell which permits controlled pressure drop/jump experiments to be conducted on a given solution in a repetitive manner. The results are presented for polyethylene + *n*-pentane solutions. Specifically, the present article provides information on the kinetics of pressure induced phase separation of polyethylene (PE 108000) from *n*-pentane solutions. It is shown that when the two-phase regions are entered rapidly, below a characteristic quench depth, the time scale for new phase growth becomes extremely short. These characteristic pressures which depend on the polymer concentration help identify a kinetic phase separation boundary which is of practical significance. Any rapid pressure-quench below this boundary results in extremely fast phase separation.

EXPERIMENTAL

Experimental system

Figure 3 shows the schematics of the overall experimental system. It consists of two optical cells, a main dissolution cell (MC) and a scattering cell (SC) which are interconnected. Other components of the system are the laser source (LS), light detectors (PMT, PD), pressure and temperature sensors (PT), a magnetic recirculation pump

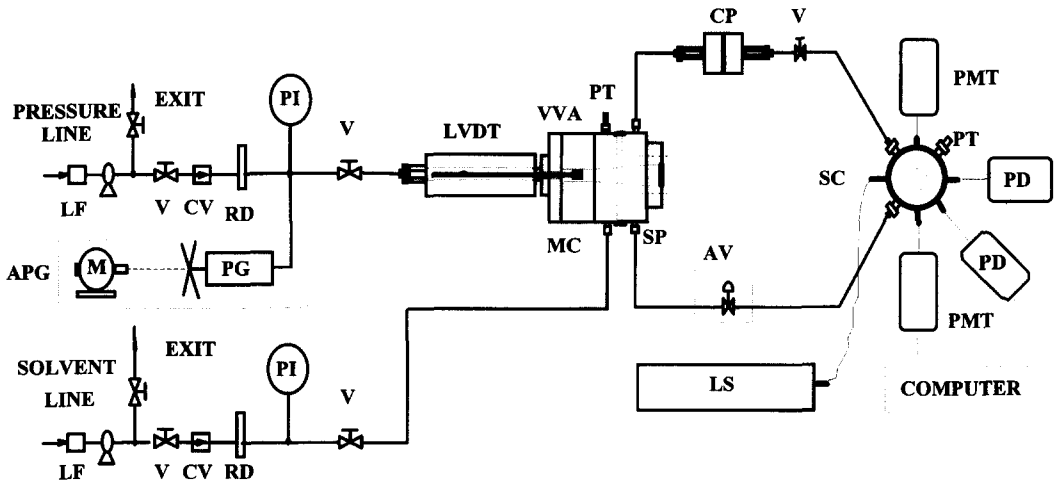

Figure 3 Experimental system to study kinetics of pressure-induced phase separation by time-resolved light scattering. (APG = automated pressure generator; AV = air-actuated valve; CP = circulation pump; CV = check valve; LF = line filter; LS = laser source; LVDT = linear variable differential transformer; M = motor; MC = main cell; PD = photo-detector; PG = pressure generator; PI = pressure indicator; PL = pressure generation line; PMT = photo-multiplier tube; PT = pressure transducer; RD = rupture disc; SC = scattering cell; SP = sample port; VVA = variable-volume assembly)

(CP), an air-actuated valve (AV), and the manifolds for solvent delivery and discharge and pressure control. Internal volume of the main cell is changed by moving a piston inside the variable-volume part (VVA) of the main cell with the aid of an automated pressure generator (PGN). The main cell along with its motorised pressure generator and the real time piston position (and thus internal volume) sensing capability (LVDT) functions also as an automated PVT apparatus[41].

Using this system pressure changes in the scattering cell are brought about repetitively without changing the solution, and the time dependent changes in the solution are followed by the time-evolution of the scattered light intensities that are monitored at different angles. The system permits changing the pressure either slowly or fast. After loading the system with the polymer and the solvent corresponding to a target concentration, fully homogeneous conditions are achieved by manipulation of the pressure and temperature while keeping the valves between the two cells open and maintaining recirculation between the cells. Then at a given temperature, moving the piston at controlled rates brings about slow pressure changes. After phase separation conditions are reached and the progress of new phase formation is monitored, the system is brought back to initial pressure for another experiment to be conducted starting again from the one-phase homogeneous conditions. For rapid pressure reductions, the valves in the connecting lines are first closed to isolate the main-cell and the scattering-cell from each other. Then the pressure in the main cell is reduced to a low value creating a pressure differential between the main cell and the scattering cell (which is maintained at the initial high pressure). Then, the air-actuated valve is quickly opened. The very rapid changes in the pressure and the scattered light intensities in the scattering cell are monitored as a function of time. For the next experiment with a different quench depth, the system is again brought back to the initial pressure. After homogenisation, the cells are once again isolated, the pressure in the main cell is reduced to a new lower value, and the valve is then opened to induce rapid phase separation in the solution inside the scattering cell. The system is thus rather unique in permitting the study of imposing different pressure quench depths on a given solution without having to reload the cells after each experiment. We refer to this technique as MRPD—Multiple Rapid (Repetitive) Pressure-Drop technique[7].

Optical cells with different geometries can be used as the scattering cell. In our previous publications we reported data obtained with a flat-window cell[6,7]. The results presented in this paper were obtained with a fibre-optic scattering cell with a very small internal volume that was designed to shorten the path lengths and reduce multiple scattering. The details of this new cell are shown in *Figure 4*. The cell, made of stainless steel, has seven ports for fibre-optic connections and a port for pressure/temperature sensor. Transmitted (0°) and scattered light from different angles with respect to the incident light can be measured with sensors attached to the fibre-optics. The dynamic changes in pressure in the scattering cell is monitored by a piezoelectric pressure transducer (PCB Piezotronics) which has a response time of 2 μs.

Optical fibres used in this set-up are glass fibre with a core diameter of 105 μm coated with polyimide for high-temperature use (obtained from SpecTran Co). To protect the thin optical fibre from physical damage and help seal in the connections, the fibres were shielded with PEEK tubing of 1/16″ o.d. and 0.007″ i.d. The tubing is then mounted onto the scattering cell and sealed. The length of the fibre extending in the cell determines the effective path length of the cell. For the present set-up, this effective length is about 2.5 mm.

In the present study, the green light of an Argon-ion laser (Lexel Model 95-AR 2) with a wave length of 514 nm has been used. Its power is adjustable and can be continually changed from 10 mW to 2 W. For the measurements in the present study a range of 10 mW has been used. Scattered light intensities were monitored using sensitive photo-multiplier tubes (PMT) or resistive photo-detectors (PD). The signal from the PMT is processed using a fast multiple-channel scaler (Stanford Instruments) with a memory storage capability of 16 000 data points. The signals from all detectors are transferred to the computer for real-time display along with system pressure and temperature.

System controls and calibrations

The overall system controls and the data acquisition protocols are built around an IBM compatible personal computer with a plug-in A/D board. This ISA bus A/D board

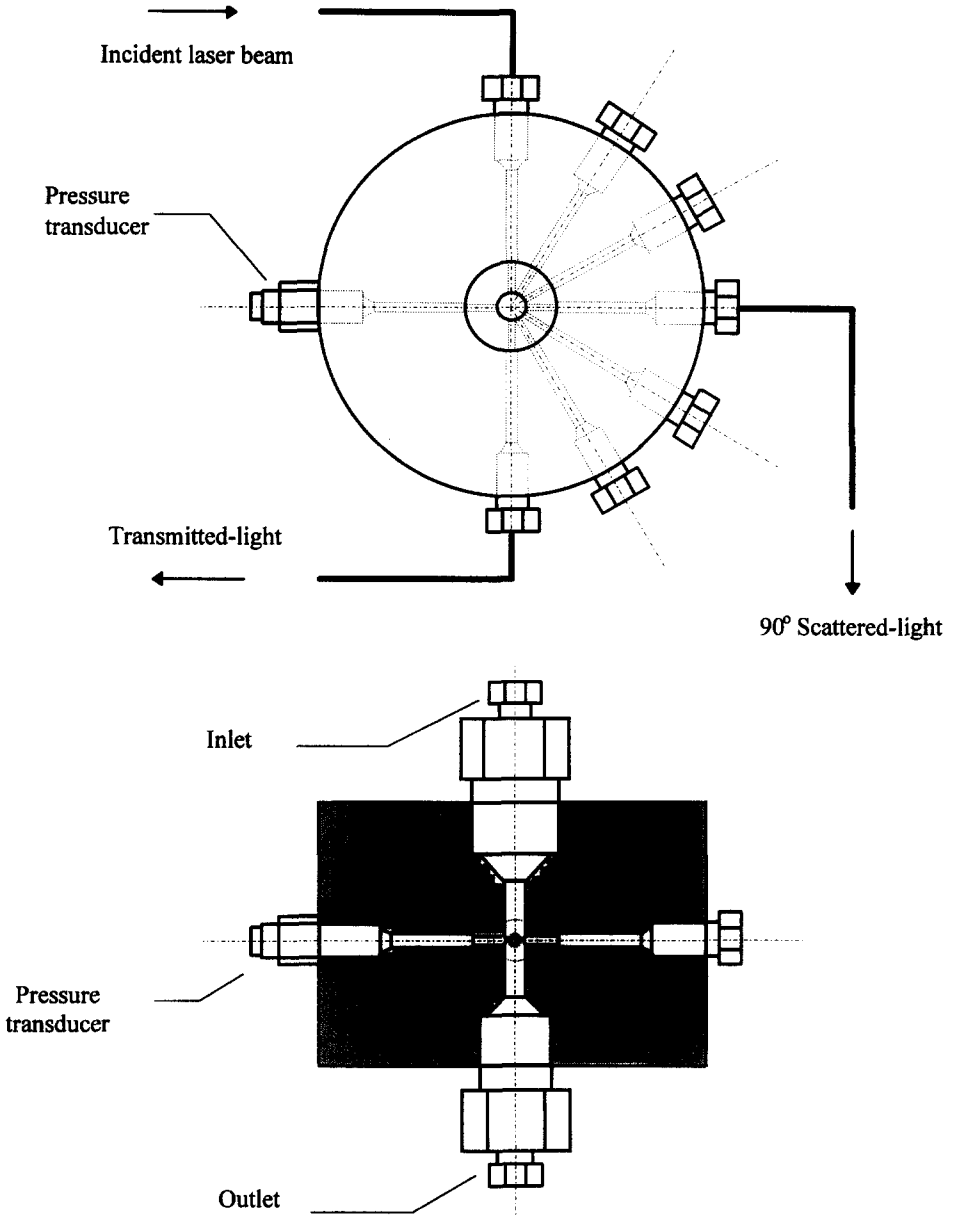

Figure 4 Schematics diagram of the fibre-optic scattering cell. The cylindrical stainless-steel cell body hosts seven ports for fibre-optic connections (incident laser beam, transmitted, (0°) and the scattered light from angles 30°, 60°, 90°, 120° and 150° with respect to the incident light) and a port for pressure/temperature sensor

has eight 12-bit differential analog input channels, two 12-bit analog outputs and one individually addressable 8-bit I/O port. The analog input channels take in the signals of the temperatures from the thermocouples (J-type) on the cells and the RTD (Pt-type) in the oven, the cell pressure from the on-line strain-gauge pressure transducer and the volume from the LVDT.

The temperature sensors (i.e. TC and RTD) are calibrated against a standard probe or a factory calibrated one by adjusting the pre-amplifier of the sensors (hardware calibration) or by fine tuning the scaling parameter in the control program (software calibration). An overall accuracy of 0.5 K and a resolution of 0.1 K is maintained. Pressure calibrations are carried out against a Heise gauge and corrections are made through adjusting the scaling parameter in the control program. In pressure readings up to 70 MPa, an overall accuracy of 0.14 MPa and a resolution of 0.017 MPa is maintained.

Calibrations of light detectors are achieved by adjusting the scaling factor in the control program while the sensor is exposed to a known light source (at low power settings of the laser).

Corrections to scattered light intensities

Corrections are made to the scattered light intensities in order to incorporate the effect of background scattering (arising from solution density fluctuations, reflections from the cell walls, or dust particles). For this purpose, scattered and transmitted light intensities are determined at homogenous one-phase conditions (far removed from the two-phase regions) where concentration fluctuations can be assumed to account for only a negligible proportion of the scattered light. Assuming that the background levels are proportional to the amount of light entering the scattering volume, following the procedures described in the literature[11], the corrected value of the scattered light intensity is obtained by subtracting the background scattering $I_{\theta b}$ from the experimentally observed value I_θ, that is,

$$I_\theta^{corr} = I_\theta - I_{\theta b}$$

where

$$I_{\theta b} = [I_\theta / I_{tr}] * I_{tr}$$

and $[I_\theta/I_{tr}]^*$ corresponds to the readings in the homogeneous region, and I_{tr} is the transmitted light intensity.

To document the changes in the scattered light intensity after a quench, the scattered light intensities are reported as normalised intensities I/I_o. The scattered light intensity I is normalised with respect to the initial scattered light intensity of the solution I_o prior to the quench.

Materials

The polyethylene standards (M_w = 108 000, M_w/M_n = 1.32 and M_w = 16 400, M_w/M_n = 1.16), hydrogenated polybutadiene samples, used in the present work were obtained from Scientific Polymer Products, Inc. The solvent, *n*-pentane (purity > 99%), was purchased from Aldrich Chemical Co.

RESULTS AND DISCUSSION

Pressure quench experiments were conducted in pure carbon dioxide, pure *n*-pentane and in solutions of polyethylene in *n*-pentane. The results are discussed below.

Pressure-induced phase separation (PIPS)—basic methodology

The basic methodology in PIPS is demonstrated in *Figure 5a* and *b*. *Figure 5a* shows the demixing pressures as a function of temperature for a polymer solution (at a given concentration) displaying LCST type behaviour such as polyethylene + *n*-pentane system. The pressure range above the demixing pressures identifies the one-phase homogeneous region. The two-phase regions (the metastable and unstable regions) for the system is entered either by reducing the pressure or by increasing the temperature. *Figure 5b* shows the demixing pressures as a function of polymer concentration at a given temperature which in practice is generated from a constant temperature cut of the demixing data (as in *Figure 5a*) obtained at different concentrations. Also shown in these figures are the spinodal curves (dotted curves) which form the boundaries for the metastable and unstable regions for the system, and typical pressure-quench paths (A–E) that may be followed.

In pressure-induced phase separation, the objective is to enter the two-phase region by reducing the pressure. Depending upon the depth of the pressure quench imposed, the system may enter its metastable or unstable region. In a recent methodology that we developed[7], we systematically map out the phase separation process in a series of pressure drop experiments each starting from the same initial pressure in the one-phase region, but ending at a progressively lower pressures in the two-phase region. More specifically, starting from a point A in the one-phase region, first a rapid pressure drop is imposed to reach a point B while monitoring the time-evolution of the scattered light intensities. The pressure of the system is then brought back to point A and now a new pressure quench is imposed to reach a point C which is at a lower final pressure. Once again the pressure is brought back to the initial pressure and the pressure quench is carried out with even lower end-pressures to a point D and finally E, while recording the scattered light intensities during each quench.

It should be noted that rapid pressure quenches are difficult to achieve isothermally. The system follows a non-isothermal, nearly adiabatic expansion path with a drop in

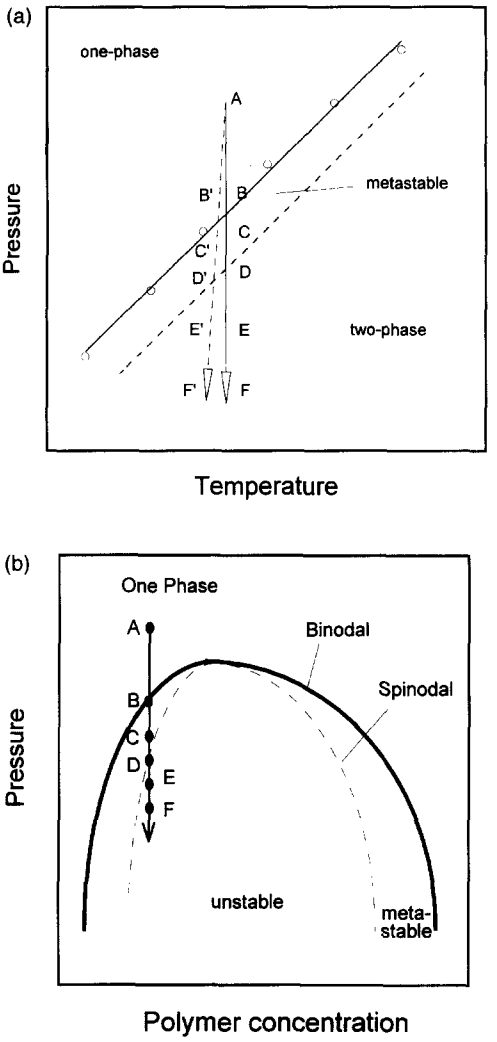

Figure 5 (a) Schematic representation of the demixing pressures (the binodal) and the spinodal phase boundary as a function of temperature for a polymer solution displaying LCST (lower critical solution temperature) type behavior. The solid line represents the demixing pressure and the dashed line represents the spinodal phase boundary. Above the demixing pressure is the one-phase homogeneous region and below is the two-phase region. Between the de-mixing pressure and the spinodal boundary is the metastable region. Two-phase regions are entered by decreasing the pressure or by increasing the temperature. The path AF represents the ideal isothermal pressure-quench path which in practice cannot be achieved. Due to adiabatic cooling, the actual path (A'F') during pressure quench will be different and will be accompanied with a decrease in temperature. (b) Schematic representations of multiple repetitive/rapid pressure drop (MRPD) technique to study kinetics of pressure-induced phase separation (PIPS) from the polymer solution. The methodology involves several pressure quench experiments, all starting from the same initial one-phase conditions (point A), but each with different penetration depth into the two-phase (metastable and unstable) regions with progressively lower final pressures, i.e. the quench paths that are followed are AB, AC, AD, AE and AF. Time evolution of scattered light intensities during each quench is monitored as an imprint of the progress of phase separation

temperature. Because the cells are in a heated oven, and because they have a large thermal mass, the actual temperature of the solutions undergoing pressure drop is in fact higher than would be anticipated from a true adiabatic expansion process. The actual paths during pressure drop experiments are schematically demonstrated in *Figure 5a*. For the present system, *Figure 6* shows the experimentally observed temperature drop in the scattering cell during a rapid pressure-quench from about 16 MPa to 6 MPa for a system which is initially maintained at about 147°C. With a 10-MPa pressure drop, which is achieved in a

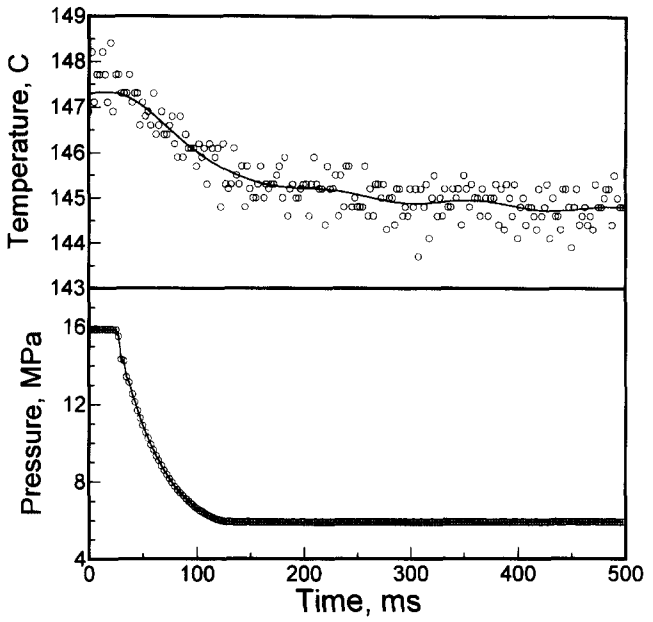

Figure 6 Experimental observation of temperature drop in the scattering cell during a rapid pressure-quench (at a rate of about 200 MPa/s) from 16 to 6 MPa. The initial temperature of the solution in the scattering cell is about 147°C

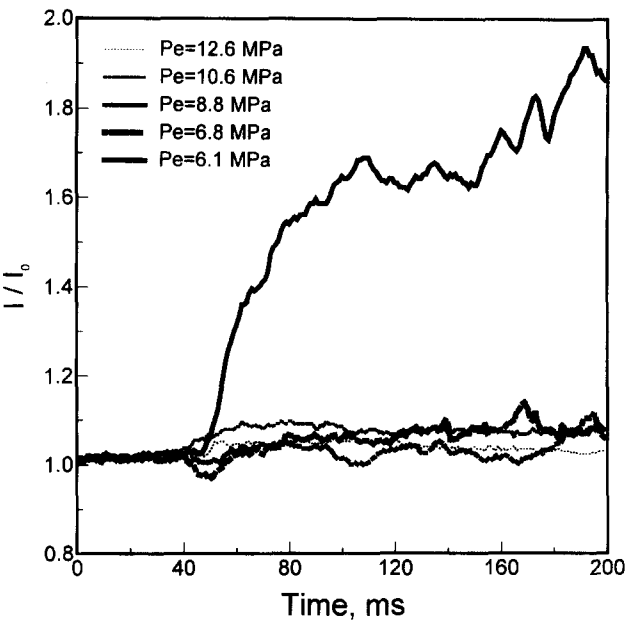

Figure 7 Evolution of scattered light intensities at 90° with time for pure carbon dioxide when subjected to different pressure quenches from an

time interval of about 50 ms, the temperature drop is observed to be about 2°C. The temperature of the cell was monitored using a special unshielded thermocouple (Omega, model IRCO-005) to minimise thermal lag and follow the temperature changes to the greatest extent possible in the time scale of the pressure changes. In all experiments conducted the total pressure quench was no greater than 10 MPa and therefore the magnitude of the actual temperature change during quench can be regarded to be less than 2°C.

The temperature effect associated with pressure-quench experiments have been well recognised in the literature in connection with phase separation in oligostyrene + pentane mixtures[10], but most extensively in connection with spinodal decomposition in binary fluid mixtures[42–51]. Temperature effect depends on the quench depth, and in a recent study with iso-butoxyethanol + water system, for a quench of 1–1.5 MPa, a temperature change of 0.2–0.4°C was reported[46]. Another factor that influences the actual temperature in a given system undergoing phase separation is the contribution from the heat of solution that should be taken into account[43,47]. Calorimetric data for polymer solutions at high pressures are rare. Even though heat of fusion and fusion temperatures have been recently reported for higher alkanes (C24-C60) and for polyethylenes at pressures up to 500 MPa[52], heat of solution data for polyethylene + *n*-pentane mixtures are not available. Thus, a priory calculation of the temperature path associated with a pressure quench path is not easy, and direct measurement of temperature is the best reliable option.

Figure 7 shows the evolution of scattered light intensities at 90° for pure carbon dioxide when subjected to different pressure quenches from an initial pressure of 14 MPa at 25°C. The pressure quenches are accomplished within 5–20 ms, and the scattered light intensities are monitored over a time interval of 200 ms. It is shown that when pressure is reduced from 14 MPa to: 12.6, 10.8, 8.8 or 6.8 MPa, the relative change in the scattered light intensity is insignificant, while for the quench to 6.1 MPa, a rapid dramatic increase is noted. The critical pressure and

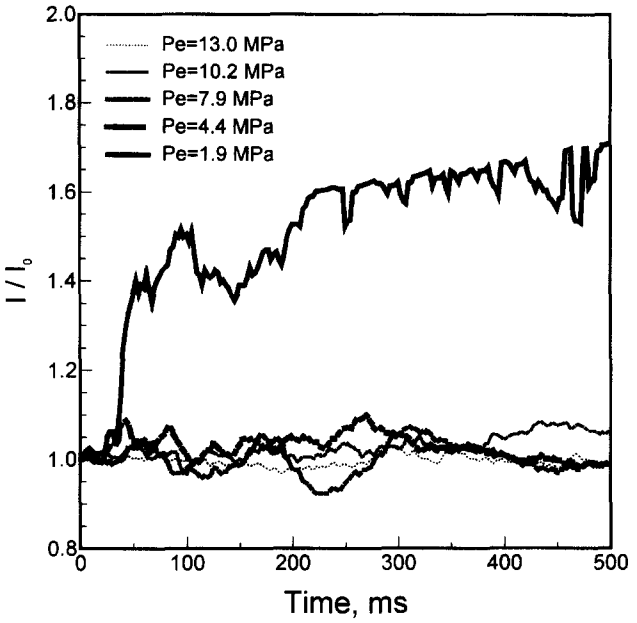

Figure 8 Evolution of scattered light intensities at 90° with time for pure *n*-pentane when subjected to different pressure quenches from an initial pressure of 14 MPa at 150°C. Final (quench) pressures are as indicated

temperature for carbon dioxide are 7.38 MPa and 31.2°C. At 25°C and 14 MPa, carbon dioxide is in the liquid state. Vapour pressure of carbon dioxide at 25°C is 6.41 MPa (and at 23°C it is 6.2 MPa)[53]. For the quench to 6.1 MPa, the vapour–liquid phase boundary has been crossed, and this phase separation process is recorded by the change in the scattered light intensities. In other quenches, the fluid remains in the liquid state. The change in density due to volume expansion shows itself only as small changes in the relative scattered light intensity.

Figure 8 shows the evolution of scattered light intensities at 90° for pure *n*-pentane when subjected to several pressure quenches to different end-pressures starting from an initial liquid state at 14 MPa and 150°C. (The critical pressure and

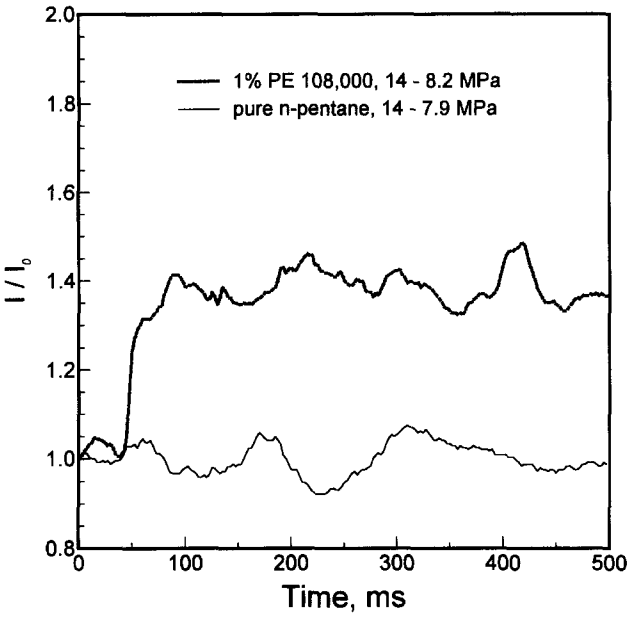

Figure 9 Comparison of the evolution of scattered light intensities at 90° of a polyethylene + *n*-pentane solution with that of pure *n*-pentane when subjected to a similar pressure quench to an end-pressure above the vapour–liquid phase boundary for *n*-pentane

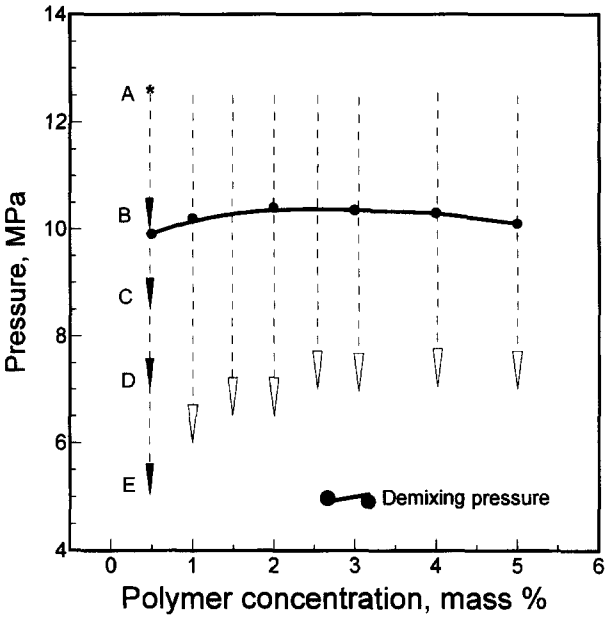

Figure 10 Quench paths for polyethylene (M_w = 108 000) + *n*-pentane polymer solutions at different polymer concentrations. The solid curve represents the actual de-mixing pressures (cloud points) at 150°C for this solution as a function of polymer concentration. The dashed lines represent multiple quenches experimentally carried out at each selected polymer concentration

temperature for *n*-pentane are 3.37 MPa and 196.6°C, respectively.) The data shows that the liquid–vapour phase boundary is crossed for the quench to 1.9 MPa. It should be noted however that the vapour pressure of pentane at 150°C is 1.58 MPa[54].

Figure 9 compares the behaviour of a polyethylene + *n*-pentane solution with that of pure *n*-pentane when subjected to a similar pressure quench to an end-pressure above the vapour–liquid phase separation boundary for *n*-pentane. It is the liquid–liquid phase separation in the polymer solution that leads to the increase in the scattered light intensity. It was important to insure that the phase-separation in the polymer solutions were being conducted in a range away from the liquid–vapour phase separation for the solvent. The behaviour of polyethylene + *n*-pentane solutions is described in detail in the following sections.

Pressure-induced phase separation in polyethylene solutions

Phase separation studies were conducted using polyethylene samples with narrow molecular weight distributions. Two polymer samples were evaluated: one with a molecular weight of 108 000 and the other 16 400.

Polyethylene (M_w = 108 000; M_w/M_n = 1.32) + n-pentane

The quench paths for this system are shown in *Figure 10*. In this figure, the solid curve represents the demixing pressures as a function of polymer concentration, determined as cloud points from slow pressure reduction experiments at 150°C[40,55]. The region above the curve represents the one-phase homogeneous region.

Following the methodology described above, at each concentration (up to 5% by mass), the solution (initially at a high pressure corresponding to a point in the one-phase region, i.e. point A) was subjected to progressively deeper pressure quenches (i.e. corresponding to pressures at points B, C, D and E).

Figures 11 and *12* show the pressure profiles and the evolution of the scattered light intensities at 90° as a function of time for a set of pressure-quench experiments for the 0.5 wt% solution from an initial pressure of 12.5 MPa. *Figure 11* shows that the pressure quenches are accomplished within about 10 ms. As shown in *Figure 12*, the scattered light intensities increase and the rate of increase becomes greater with increased quench depth, i.e. with lowered end-pressures. In *Figure 12*, scattered light intensities are shown over a total observation time of 20 s. *Figure 13* shows the results of a repeat set of quench experiments with similar end pressures, with a shorter total observation time of 2 s. In these figures, the solid curves are the smoothed curves.

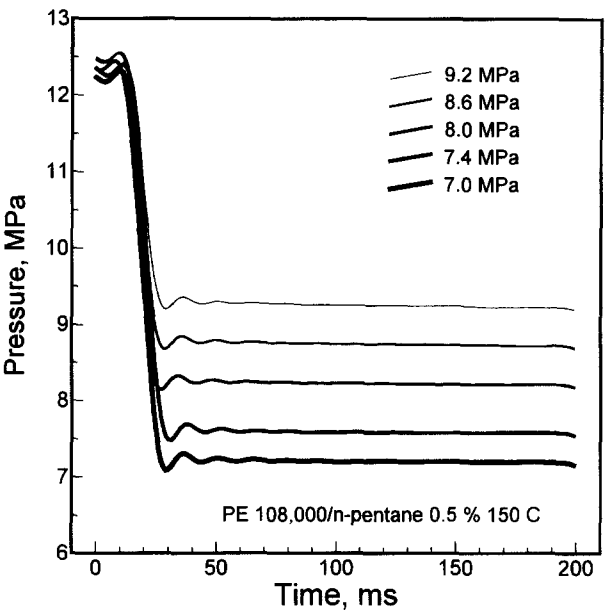

Figure 11 Pressure profiles of the multiple pressure quenches as a function of time for the 0.5% polyethylene (M_w = 108 000) + *n*-pentane solution from an initial pressure of 12.5 MPa at 150°C

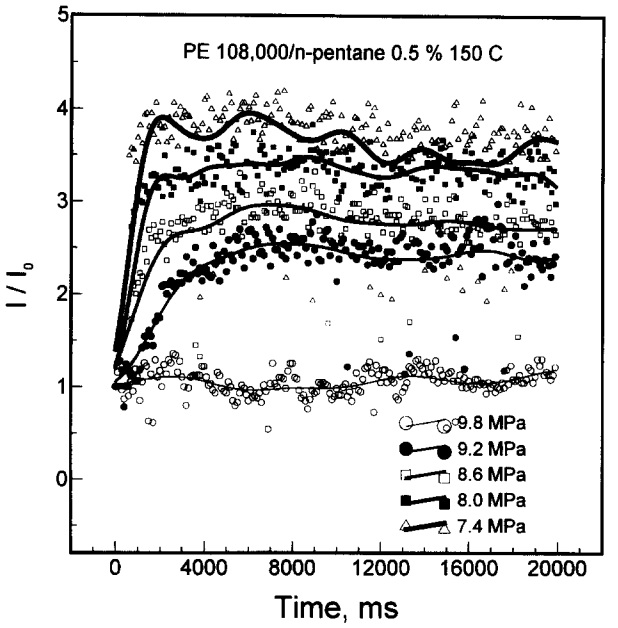

Figure 12 Evolution of the scattered light intensities at 90° for a set of multiple pressure quenches in 0.5% polyethylene (M_w = 108 000) + *n*-pentane solution from an initial pressure of 12.5 MPa at 150°C. Final pressures are as indicated (see *Figure 11*). Observation time is 20 s. The solid curves are the smoothed curves

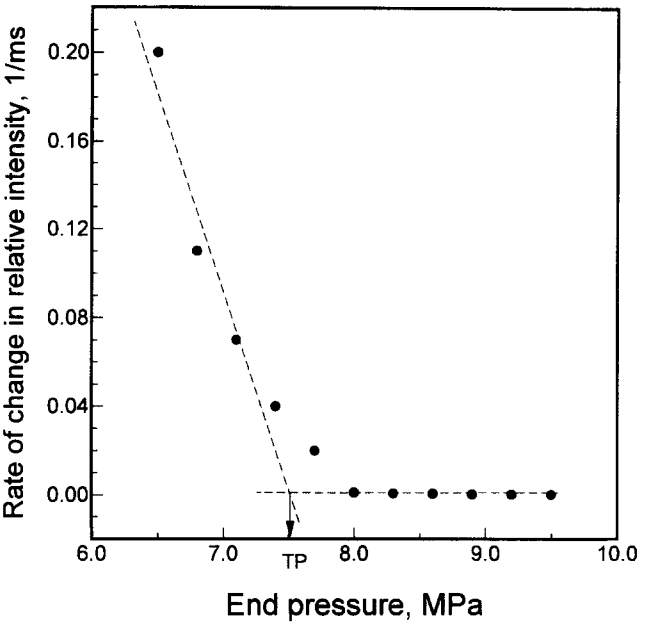

Figure 14 Rate of change of scattered light intensities with time (the slopes of the initial relative scattered intensity profiles) as a function of the end-pressure of pressure quenches which defines a characteristic end pressure, i.e. the transition pressure, TP. At pressures below this transition pressure, phase separation proceeds extremely rapidly

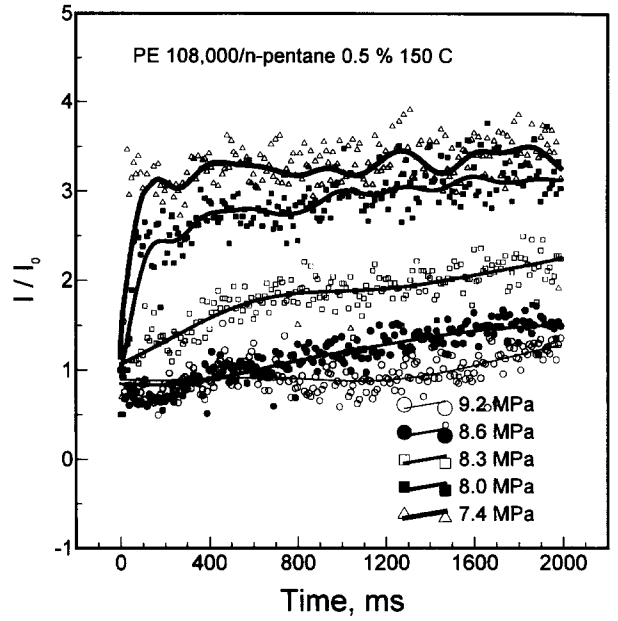

Figure 13 Evolution of the scattered light intensities at 90° for a set of multiple pressure quenches in 0.5% polyethylene (M_w = 108 000) + *n*-pentane solution from an initial pressure of 12.5 MPa at 150°C. Final pressures are as indicated. Observation time is 2 s. The solid curves are the smoothed curves

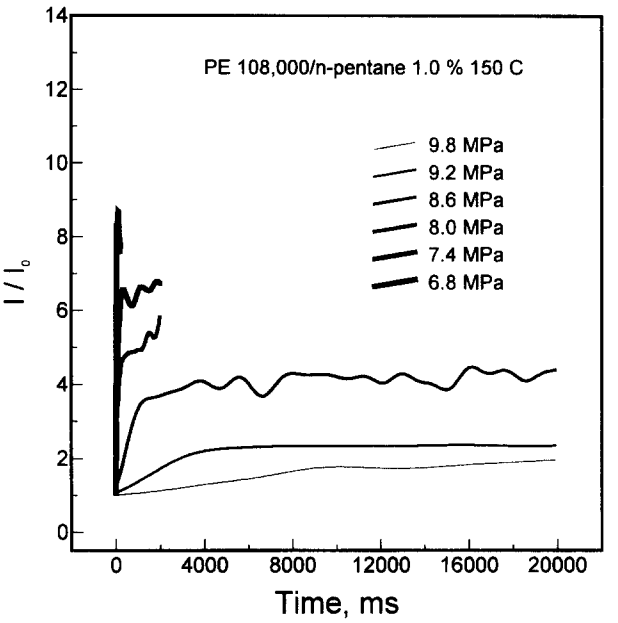

Figure 15 Evolution of the scattered light intensities at 90° for a set of multiple pressure quenches in 1% polyethylene (M_w = 108 000) + *n*-pentane solution from an initial pressure of 12.5 MPa at 150°C. Final pressures are as indicated

As can be seen from *Figure 10*, the phase boundary for this solution is about 9.6 MPa. *Figures 12* and *13* show that the changes in the scattered light intensity are indeed insignificant for a quench to 9.8 MPa which is above the cloud point pressure, but becomes large for quenches to 9.2 MPa and lower pressures.

A relatively simple approach to evaluate and compare the dependence of the phase separation process on the quench depth is to compare the rate of change of scattered light intensities with time. The slopes of the initial (short-time) relative scattered intensity profiles for this solution have been evaluated. In *Figure 14*, they are shown as a function of the end-pressure reached. From such a plot, a characteristic end pressure below which there is a dramatic increase in the rate of change of scattered light intensity in pressure-induced phase separation can be identified. This transition pressure where the time scale of phase separation shows a remarkable change is noted as TP in *Figure 14*. At pressures below this 'transition' pressure, phase separation is extremely rapid.

For this polymer + solvent system, the pressure-quench experiments were conducted also at higher polymer concentrations and the scattered light intensities were monitored and analysed by similar procedures. *Figure 15*

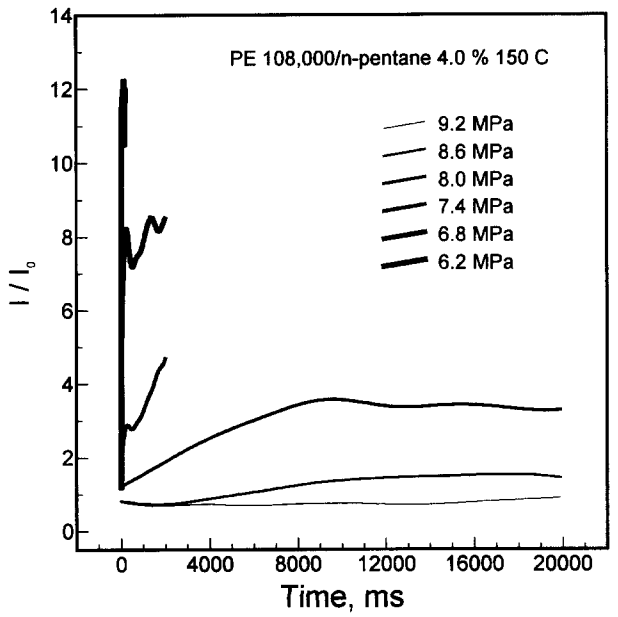

Figure 16 Evolution of the scattered light intensities at 90° for a set of multiple pressure quenches in 4% polyethylene (M_w = 108 000) + *n*-pentane solution from an initial pressure of 12.5 MPa at 150°C. Final pressures are as indicated

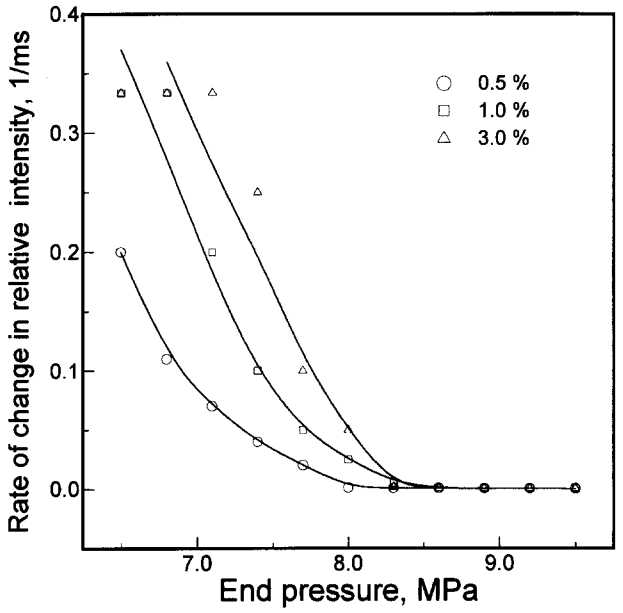

Figure 17 Rate of change in relative scattered light intensities as a function of the depth (end-pressure) of pressure quenches for polyethylene (M_w = 108 000) + *n*-pentane solutions at 150°C. Solution concentrations are as indicated

and *Figure 16* show the smoothed scattered light intensity profiles for the 1 and 4%. For shallow quenches, the data collection interval was 20 s, but for deeper quenches, in order to collect more data points to capture the fast changes, total observation times were reduced to 2 s or less. The rate of change of scattered light intensities are shown in *Figure 17* as a function of the quench pressure for solutions at 0.5, 1 and 3% concentrations. The transition pressures for extremely rapid phase separation were determined at each concentration. These pressures identify a kinetic boundary inside the two-phase region below which the system undergoes very rapid phase separation. The cloud point pressures and the inner transition pressures obtained from

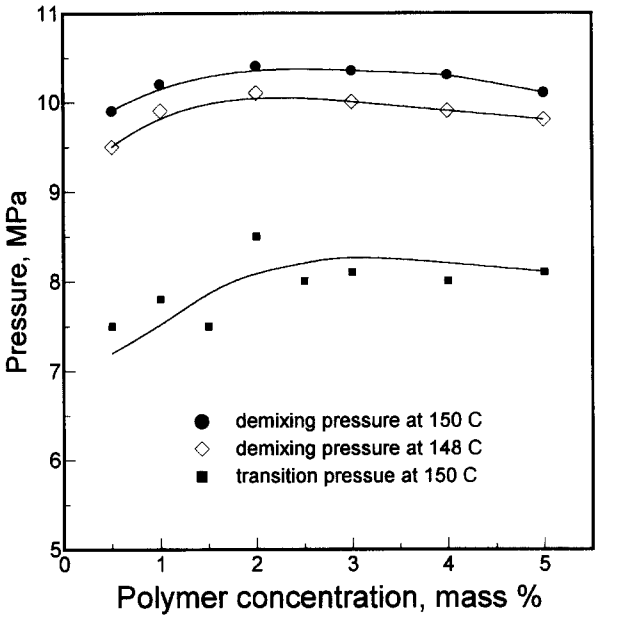

Figure 18 Comparisons of de-mixing pressure and dynamic transition pressure as obtained by the multiple pressure quench approach for polyethylene (M_w = 108 000) + *n*-pentane solution at different polymer concentrations. The de-mixing pressures at 148°C are included to account for the cooling effect (which is ~2°C, shown in *Figure 6*) in the course of rapid pressure reduction

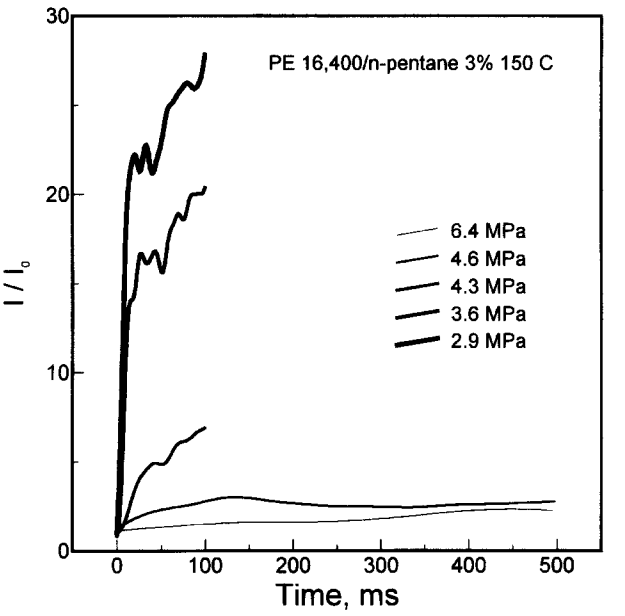

Figure 19 Evolution of the scattered light intensities at 90° for a set of multiple pressure quenches in 3% polyethylene (M_w = 16 400) + *n*-pentane solution from an initial pressure of 6.9 MPa at 150°C. Final pressures are as indicated

pressure quench experiments are shown in *Figure 18*. This inner boundary is a kinetic phase boundary of practical significance.

Polyethylene (M_w = *16 400;* M_w/M_n = *1.16) + n-pentane*

Figures 19 and *20* are representative plots of the change in relative scattered light intensity at 90° with time for this system upon pressure quench to different end-pressures. The results are shown for 3 and 5% solutions at 150°C. Similar experiments were conducted at several other concentrations. The transition pressures for each system

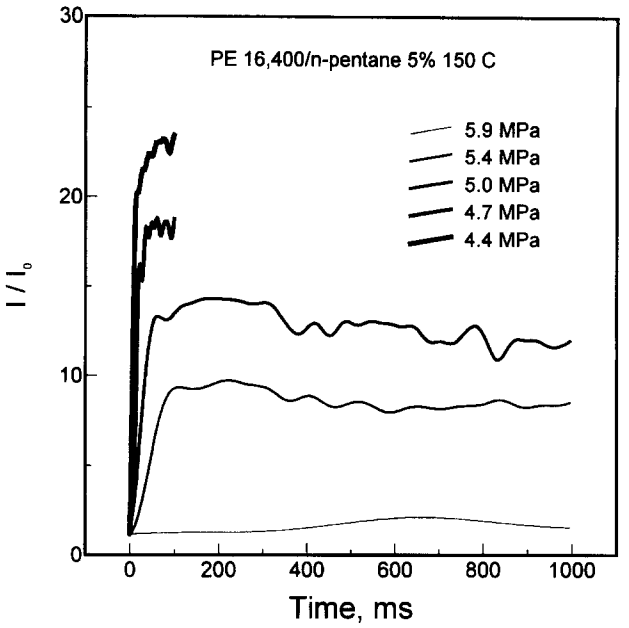

Figure 20 Evolution of the scattered light intensities at 90° for a set of multiple pressure quenches in 5% polyethylene ($M_w = 16\,400$) + *n*-pentane solution from an initial pressure of 6.9 MPa at 150°C. Final pressures are as indicated

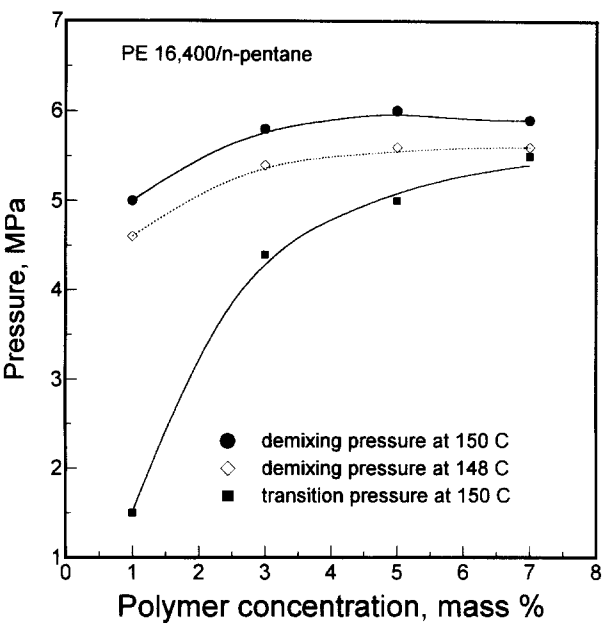

Figure 22 Comparisons of de-mixing pressure and the dynamic transition pressure as obtained by the multiple pressure quench approach for polyethylene ($M_w = 16\,400$) + *n*-pentane solution at different polymer concentrations. The de-mixing pressures at 148°C are also included to permit comparisons on account of the cooling effect in the course of rapid pressure reduction

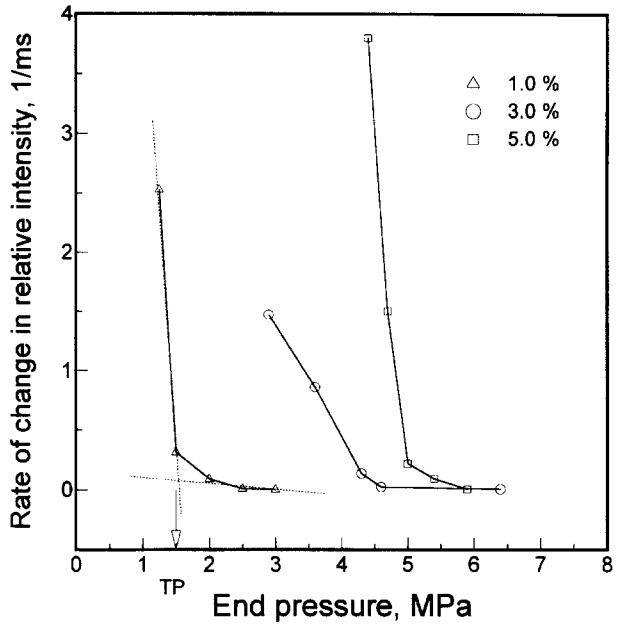

Figure 21 Rate of change in relative scattered light intensities as a function of the depth (end-pressure) of pressure quenches for polyethylene ($M_w = 16\,400$) + *n*-pentane solutions for different polymer concentrations at 150°C

were then determined from plots of the rate of change in relative scattered light intensity *versus* end-pressure of the quench as shown in *Figure 21*. *Figure 22* compares the cloud point pressures for this system with the inner, dynamic phase-separation boundary.

Further discussion

The present observations show the transition in the kinetics of phase separation with the quench depth imposed. A distinct change in the scattered light intensity with quench depth has also been reported in a series of temperature quench experiments conducted in mixtures of styrene oligomers and ϵ-caprolactone[27]. The scattered light intensity in that system is reported to be much lower in the nucleation and growth regime than the spinodal decomposition regime if compared at the same phase-separation time. The speed of phase separation increases with an increase in quench depth and shows a sharp demarcation around the transition from metastability to unstability. One is therefore tempted to make the suggestion that the kinetic phase boundary reported in the present study may be indicative of a change in the mechanism of phase separation from nucleation and growth to spinodal decomposition. However, as demonstrated in *Figure 5b*, the thermodynamic spinodal boundary should in principle merge with the binodal curve at the critical polymer concentration. The critical polymer concentration for this polymer + solvent system was not experimentally determined. Predictions by Sanchez–Lacombe and SAFT models after fitting the experimental demixing pressures suggests a critical concentration of about 2% by mass for the polymer with $M_w = 108\,000$ and at about 5% for the polymer with $M_w = 16\,400$[56,57]. For polymers with polydispersity, the actual critical concentration is often shifted to higher concentrations.

Figures 18 and *22* show that the dynamic inner boundary, as determined in the present study, does not merge with the binodal in the concentration range evaluated and thus does not meet the criteria for thermodynamic spinodal boundary. However, recent studies by Tanaka[58,59] indicate that in deep quench experiments involving asymmetric systems such as polymer solutions, the phase separation process may be strongly affected by elastic effects, and such systems may show a dynamic symmetry line and undergo viscoelastic spinodal decomposition. Tanaka suggests that when the characteristic deformation time is shorter (as would be the case in rapid deep quenches) than the characteristic rheological time, polymer solutions behave like elastic gels (due to entanglements). In contrast, they behave like viscous fluids for slower deformations. For a deep quench, a large difference is expected in the dynamics between the

two co-existing phases (an elastic or transient network characterised by slow dynamics and a fluid characterised by fast dynamics) and visco-elastic effects may play a dominant role in the progress of phase separation. The elastic effects are presumed to suppress the enhancement of concentration fluctuations which is characteristic of the initial stage of spinodal decomposition. In systems influenced by elastic effect, the elastic energy barrier must be overcome for the phase separation to proceed. Tanaka further argues that in such systems, phase separation may proceed by nucleation and growth in the less elastic phase even for an unstable state and move the spinodal boundary. The present observations could perhaps be perceived as being in line with these arguments considering the very rapid quench rates and deep quenches that are imposed.

Another factor that needs to be considered is the shift in the location of the binodal with temperature. As pointed out earlier, these rapid pressure quenches are accompanied with a change in the temperature of the solution and in the present study experimentally observed change is about 2°C or lower. Since the polyethylene + *n*-pentane system shows LCST type behaviour, lowering the temperature will lower the demixing pressures and move the binodal to a lower boundary. In *Figure 18*, the cloud point curve for a solution at 148°C is also included. Compared to the cloud point curve at 150°C, this curve represents the location of the boundary for the case with the 2°C cooling as actually monitored. The kinetic phase boundary is clearly at much lower pressures than can be attributed to a simple temperature dependent shift in the binodal, unless the temperature shift is much greater and occurs at a rate faster than can be recorded. The inner boundary may be reflecting a change in mechanism of phase separation. If this boundary were representative of the spinodal boundary, it would be the boundary corresponding to a lower temperature than the initial temperature of the solution. As such, it would be more appropriate to compare it with the binodal boundary corresponding to the lower temperature. The downshift movement of the binodal with cooling is in the right direction towards improving the possibility for merging of the spinodal and the binodal at the critical polymer concentration.

For systems undergoing spinodal decomposition, typically conducted at the critical polymer concentration imposed to shallow pressure quenches, scattered light intensity is known to increase with time and go through a maximum with scattering angle. If it follows the linearised Cahn–Hilliard Theory[22–24,38,60,61], the angle at which the maximum in the scattered light intensity is observed is a time invariant and the scattered light intensity grows exponentially in time according to

$$\ln I(q, t) = \ln I(q, 0) + 2R_q t \quad (1)$$

where R_q is the rate constant and, q is the scattering vector and defined as

$$q = (4\pi/\lambda) \sin(\theta/2) \quad (2)$$

where λ is the wavelength of the light and θ is the scattering angle. For polymer solutions the intensity maximum is observed at low angles, typically below 15°.

In the present system, the scattered light intensities could not be measured at such low angles and the presence or absence of a maximum of scattered intensity with scattering angle, and whether or not q_m is time invarient as would be predicted by the linearised Cahn–Hilliard formalism could not be discerned for the rapid deep-quench experiments.

Current research in our laboratory is focused on the low angle measurements for further elucidation of the change in mechanism and the spinodal process under shallow and deep-quench experiments. Shallow pressure-quench experiments conducted in polystyrene + methyl cyclohexane at the critical polymer concentration in a flat-window scattering cell which permits monitoring the scattering intensities at low angles display all the well-known aspects of spinodal decomposition with respect to angular variation of scattered light intensities[13,62]. However, for rapid and deep quenches similar to those described in the present study, the dynamics to be monitored by the sampling rates accessible with commercial linear image sensors become very fast and the scattering maximum cannot be captured even at critical polymer concentrations. These observations further the notion that in rapid quench experiments the dynamics of phase separation may display different characteristics. We are exploring alternative approaches to document the extremely short time (i.e. microsecond) processes.

Conclusions

Pressure-induced phase separation in polymer solutions can be conveniently followed using a dual cell optical system. Rapid pressure-quench experiments in polymer solutions identify a kinetic phase boundary below the de-mixing pressures. This boundary is a dynamic phase boundary below which phase separation processes are extremely rapid.

REFERENCES

1. Nishi, T., Wang, T. T. and Kwei, T. K., *Macromolecules*, 1975, **8**, 227.
2. Snyder, H. L. and Meakin, P. J., *Polym. Sci., Polymer Symp.*, 1985, **73**, 217.
3. Inoue, T. and Ougizawa, T. J., *Macromol. Sci. -Chem.*, 1989, **A26**(1), 147.
4. Lloyd, D. R. , Kinzer, K. E. and Tseng, H. S., *J. Membrane Sci.*, 1990, **52**, 239.
5. Nelson, D. S. and Soane, D. S., *Polym. Eng. Sci.*, 1993, **33**, 1619.
6. Kiran, E., in *Supercritical Fluids—Fundamentals for Application*, ed. E. Kiran and J. M. H. Levelt Sengers. Kluwer Academic Publishers, Dordrecht, The Netherlands, 1994.
7. Kiran, E. and Zhuang, W., *J. Supercrit. Fluids*, 1994, **7**, 1.
8. Zhuang, W. and Kiran, E., *Proceedings of the 1st Joint Topical Conference on Processing, Structure and Properties of Polymeric Materials*, AIChE, New York, 1996.
9. Kiran, E. and Zhuang, W., in *Supercritical Extraction*, ed. M. Abraham and A. K. Sunol. ACS Symposium Series 670, Washington, DC, 1997.
10. Kiepen, F. and Borchard, W., *Macromolecules*, 1988, **21**, 1784.
11. Wells, P. A., deLoos, Th. W. and Kleintjens, L. A., *Fluid Phase Equilibria*, 1993, **83**, 383.
12. Goel, S. K. and Beckman, E. J., *Polymer Eng. Sci.*, 1994, **34**, 1137.
13. Kiran, E., in *Proc. the 4th International Symposium on Supercritical Fluids*, Vol. C, Sendai, Japan, 11–14 May 1997, pp. 777–784.
14. Lin, F.-C., Wang, D.-M. and Lai, J.-Y., *J. Membrane Sci.*, 1996, **109**, 93.
15. Koros, W. J. and Pinnau, I., in *Polymeric Gas Separation Membranes*, ed. D. Paul and Y. P. Yampol'skii. CRC Press, Boca Raton, 1994, p. 209.
16. Dixon, D. J. and Johnston, K. P., *J. Appl. Poly. Sci.*, 1993, **50**, 1929.
17. Dixon, D. J., Johnston, K. P. and Bodmeier, R. A., *AIChE J.*, 1993, **39**, 127.
18. Ryan, A. J., *Polymer*, 1990, **31**, 707.
19. Okada, M., Fujimoto, K. and Nose, T., *Macromolecules*, 1995, **28**, 1795.
20. Chan, C. K., Perrot, F. and Beysens, D., *Phys. Rev. A*, 1991, **43**, 1826.

21. Hashimoto, T., Takeba, T. and Fujioka, K., in *Dynamics and Patterns in Complex Fluids*, ed. A. Onuki and K. Kawasaki. Springer, Berlin, 1990.
22. Hashimoto, T., *Phase Transitions*, 1988, **12**, 47.
23. Han, C. C. and Akcasu, A. Z., *Annu. Rev. Phys. Chem.*, 1992, **43**, 61.
24. Perrault, F. and Prud'homme, R. E., *Polm. Eng. Sci.*, 1995, **35**, 34.
25. Smolders, C. A., von Aartsen, J. J. and Steenbergen, A., *Kolloid-Z. Z. Polm.*, 1971, **243**, 14.
26. Nojima, S., Tsutsumi, K. and Nose, T., *Polymer J.*, 1982, **14**, 225.
27. Tanaka, H., Yokokawa, T., Abe, H., Hayashi, T. and Nishi, T., *Phys. Rev. Lett.*, 1990, **65**, 3136.
28. Tanaka, H. and Sigehuzi, T., *Phys. Rev. Lett.*, 1995, **75**, 874.
29. Lal, J. and Bansil, R., *Macromolecules*, 1991, **4**, 290.
30. Aubert, J. H. and Clough, R. L., *Polymer*, 1985, **26**, 2047.
31. Aubert, J. H., *Macromolecules*, 1988, **21**, 3469.
32. Tanaka, H., *Phys. Rev. Lett.*, 1993, **71**, 3158.
33. Song, S.-W. and Torkelson, J. M., *Macromolecules*, 1994, **27**, 6389.
34. McGuire, K. S., Laxminarayan, A. and Lloyd, D. R., *Polymer*, 1995, **36**, 4951.
35. Kikuchi, H., Usui, F. and Kajimaya, T., *Polymer J.*, 1996, **28**, 35.
36. Xie, Y., Ludwig, K. F., Bansil, R., Gallagher, P. D., Konak, C. and Morales, G., *Macromolecules*, 1996, **29**, 6150.
37. Kojima, J., Nakayama, Y., Takenaka, M. and Hashimoto, T., *Rev. Sci. Instrum.*, 1995, **66**, 4066.
38. Kuwahara, N. K. and Kubota, K., *Phys. Rev. A*, 1992, **45**, 7385.
39. Kuwahara, N., Hamano, K., Aoyama, N. and Nomura, T., *Phys. Rev. A.*, 1983, **27**, 1724.
40. Zhuang, W., Ph.D. thesis, University of Maine, Orono, ME, 1995.
41. Zhuang, W. and Kiran, E., *Rev. Sci. Instrum.*, 1996, **67**, 244.
42. Wong, N.-C. and Knobler, C. M., *J. Chem. Phys.*, 1978, **69**(2), 725.
43. Metz, U. and Schneider, G. M., *Ber. Bunsenges. Phys. Chem.*, 1990, **94**, 447; 1990, **94**, 452.
44. Clerke, E. A. and Sengers, J. V., *Physica*, 1983, **118A**, 360.
45. Sieber, M. and Woermann, D., *Ber. Bunsenges. Phys. Chem.*, 1991, **95**, 15.
46. Bailey, A. E. and Cannell, D. S., *Phys. Rev. Lett.*, 1993, **70**, 2110.
47. Donley, J. P. and Langer, J. S., *Physica A*, 1994, **204**, 202.
48. Steinhoff, B. and Woermann, D., *J. Chem. Phys.*, 1995, **103**, 8985.
49. Schneider, G. M., *Pure & Appl. Chem.*, 1991, **63**, 1313.
50. Schneider, G. M., Dittman, M., Metz, U. and Wenzel, J., *Pure & Appl. Chem.*, 1987, **59**, 79.
51. Yamamura, O., Takahara, S. and Suga, H., *J. Non-Cryst. Solids*, 1995, **183**, 144.
52. Hohne, G. W. H. and Blankhorn, K., *Thermochimica Acta*, 1994, **238**, 351.
53. Angus, S., Armstrong, B. and deReuck, K. M. (ed.), *International Thermodynamic Tables of the Fluid State. Carbon Dioxide.* Pergamon, New York, 1976.
54. Vargaftic, N. B., *Tables on the Thermophysical Properties of Liquids and Gases*, 2nd edn. Wiley, New York, 1975.
55. Kiran, E. and Zhuang, W., *Polymer*, 1992, **33**, 5259.
56. Kiran, E., Xiong, Y. and Zhuang, W., *J. Supercrit. Fluids*, 1993, **6**, 193.
57. Xiong, Y. and Kiran, E., *J. Appl. Polym. Sci.*, 1995, **55**, 1805.
58. Tanaka, H., *J. Chem. Phys.*, 1994, **100**(7), 5323.
59. Tanaka, H., *Int. J. Thermophys.*, 1995, **16**, 371.
60. Cahn, J. W., *Acta Metal.*, 1961, **9**, 795.
61. Cahn, J. W., *J. Chem. Phys.*, 1965, **42**, 93.
62. Xiong, Y., Ph.D. thesis, University of Maine, Orono, ME, in preparation.